Optical rogue waves in multifractal photonic arrays

F. Sgrignuoli[1], Y. Chen[1], S. Gorsky,[1] W. A. Britton,[2] and L. Dal Negro[1,2,3,*]

[1]*Department of Electrical and Computer Engineering, Boston University, 8 Saint Mary's Street, Boston, Massachusetts 02215, USA*
[2]*Division of Materials Science and Engineering, Boston University, 15 Saint Mary's Street, Brookline, Massachusetts 02446, USA*
[3]*Department of Physics, Boston University, 590 Commonwealth Avenue, Boston, Massachusetts 02215, USA*

Optical rogue waves are demonstrated in the far-field scattered radiation from photonic arrays designed according to the aperiodic distributions of prime elements in complex quadratic fields. Specifically, by studying light diffraction from Eisenstein and Gaussian prime arrays, we establish a connection between the formation of optical rogue waves and multifractality in the visible single-scattering regime. We link strong multifractality with the heavy-tail probability distributions that describe the fluctuations of scattered radiation from the fabricated arrays. Our findings pave the way to control high-intensity rogue waves using deterministic arrays of dielectric nanostructures for enhanced sensing and lithographic applications.

I. INTRODUCTION

The term "rogue waves" (RWs) was originally introduced in hydrodynamics to describe the behavior of giant waves that emerge unexpectedly on a relatively calm ocean releasing exceptionally destructive power [1]. Since then, RWs have been observed in different contexts (e.g., optics [2–8], condensed-matter physics [9], optical turbulence [10], and even in finance [11], to cite a few), becoming an important subject of interdisciplinary research [2,3,12].

Despite the theoretical and experimental efforts of the past 12 years [2,3,13], an exact definition of a RW does not exist yet [12]. Moreover, as pointed out in recent reviews [2,3], the analogy between optical and ocean rogue waves must be handled with care. However, a common feature of all these studies is the presence of heavy-tailed probability density functions (PDFs) describing the intensity fluctuations of the waves. Therefore, RWs are characterized by non-Gaussian statistics, implying that waves with extremely large amplitudes appear more often than what is predicted from the normal distribution. Heavy-tailed statistical distributions arise in the context of extreme value theory (EVT) beyond the validity of the central limit theorem when limit processes, such as the sum of dependent and correlated variables, are considered [14,15]. Fundamental aspects of the physics of optical RWs are the presence of heavy-tailed PDFs in the statistical distribution of scattered radiation and its connection with the structural properties of complex systems. However, the mechanisms driving the formation of RWs is a matter of debate and depends on the particular system under study [1,3,16,17].

Recently, Dematteis *et al.* proposed and tested a statistical theory demonstrating that water tank rogue waves are hydrodynamic instantons [18]. Instead, optical RWs were demonstrated for the first time by Solli *et al.* in microstruc-

tured optical fibers driven within a noise-sensitive nonlinear regime [4]. The strong phase gradients and fluctuations that give rise to natural focusing phenomena [19], described by the theory of catastrophe optics [20,21], also produce abrupt, rare, and extreme fluctuations of field amplitudes. These studies established a connection between rogue-type behavior and far-field diffracted caustics [7,8,22]. Moreover, these discoveries showed that nonlinearity is not essential for the generation of optical RWs that can be observed in linear systems when a suitable random phase structure is imparted on a coherent optical field [6–8] or when disordered phases exhibit long-range correlations in space [23]. Wave focusing due to collective effects in a correlated complex medium [15], granularity, and spatial inhomogeneity [5,17] have been identified as the main factors for the occurrence of RWs in the optical regime.

In this work, we propose and demonstrate an approach for the generation of optical RWs based on the engineering of deterministic arrays of dielectric nanostructures with aperiodic multifractal geometry [24]. Multifractals, i.e., intertwined sets of self-similar structures, are inhomogeneous systems characterized by complex fluctuations over multiple-length scales that encode long-range correlations [19]. Introduced by Frisch and Parisi to analyze the multiscale energy dissipation in turbulent fluids [24], multifractality (MF) became an interdisciplinary concept that is investigated in various fields of research. Besides finance [25], chaotic systems [26], and condensed-matter physics [27], self-similarity and multifractality have been observed in soliton-based systems [28]—like the ones used to demonstrate optical RWs (see, e.g., [2] and references therein)—and in extremely rare natural hazards [19], such as tsunami [29], earthquakes [30], and oceanographic rogue waves [31]. Interestingly, also diffracted caustics, as pointed out by Berry and Upstill [22], are characterized by a hierarchy of self-similar lengthscales.

Motivated by these findings, we ask whether a fundamental connection exists between MF and RWs in linear optics. To establish such a relation, we measured the diffraction intensity

*dalnegro@bu.edu

195403-1

patterns produced by aperiodic photonic arrays designed from fundamental structures of algebraic number theory [32–35] that inherit the multifractality of the distributions of prime elements [36]. The multifractality of these photonic systems has been demonstrated in Ref. [32] in the multiple scattering regime by performing leaky-mode imaging experiments at high numerical aperture. Instead, in the present work we systematically investigate their single-scattering properties, focusing on the far-field diffracted radiation from Eisenstein and Gaussian prime arrays. First of all, we demonstrate that the structure factor of these arrays, which is proportional to the far-field scattered intensity [37], exhibits strong multifractal behavior. As a second step, we show that the PDFs of scattered radiation, which characterize the spatial fluctuations of coherent laser light diffracted by the aperiodic structures, as well as the distributions of the most intense values, are described by Pareto-type and Fréchet-type extreme value distributions, respectively. Finally, we determine that these non-Gaussian statistics originate from the strong multifractal geometry of the investigated photonic arrays.

II. MULTIFRACTAL DIFFRACTION OF PRIME ARRAYS

The photonic structures are fabricated using electron beam lithography. Specifically, TiO_2 nanocylinders deposited atop a transparent SiO_2 substrate are arranged as the prime elements of the Eisenstein and Gaussian integers. Recently, these photonic arrays were introduced to exploit structural multifractality as an engineering approach for optical sensing, lasing, and multispectral devices [32,33]. Scanning electron microscope (SEM) images of the fabricated devices are reported in Figs. 1(a) and 1(b). More details on the fabrication as well as on their geometrical properties are discussed in Ref. [32] and in the Supplemental Material [38]. The experimental setup used to measure the diffraction pattern of laser light scattered by the arrays is shown in Fig. 1(c). A 405 nm laser is focused onto the device to uniformly illuminate the sample. The forward scattered light is collected by a high numerical aperture objective (NA=0.9 Olympus MPlanFL N) that gathers light scattered up to 64° from the normal direction. Immediately behind the objective, a 4-F optical system creates an intermediate image plane and an intermediate Fourier plane. An iris, located at the intermediate image plane, was used to restrict the light collection area only to the patterned regions. The intermediate Fourier plane was reimaged onto a charge-coupled device (CCD) with the appropriate magnification by using a second 4-F optical system. Finally, digital filtering was employed to remove the strong direct component of the diffraction spectra to produce the clear images reported in Figs. 1(d) and 1(e) for the Eisenstein and Gaussian configurations, respectively. The experimental results are compared with the predicted far-field diffraction intensity that is proportional to the computed structure factor of the investigated arrays, defined as [32,37]

$$S(\boldsymbol{k}) = \frac{1}{N} \left| \sum_{j=1}^{N} e^{-i\boldsymbol{k} \cdot \boldsymbol{r}_j} \right|^2, \qquad (1)$$

where $\boldsymbol{k}$ is the in-plane component of the wave vector, and $\boldsymbol{r}_j$ are the vector positions of the N nanoparticles in the array.
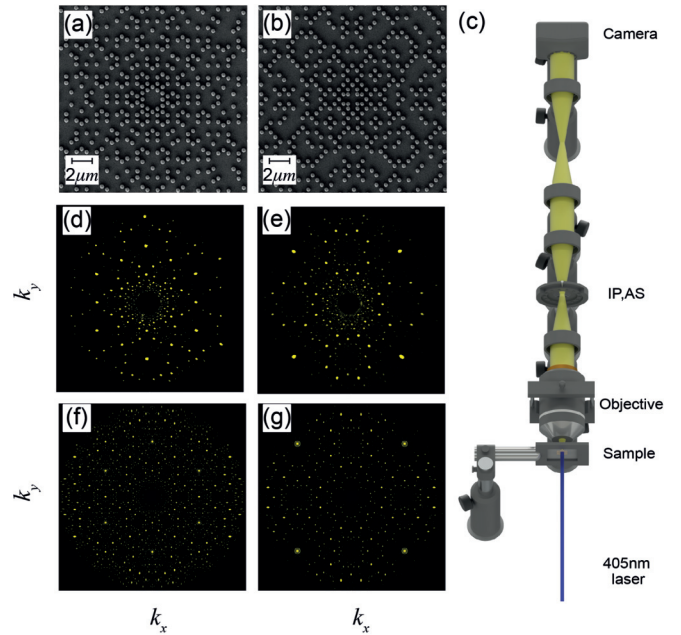

FIG. 1. SEM images of the fabricated photonic arrays arranged in an Eisenstein (a) and Gaussian (b) geometry, respectively. Nanocylinders have a 210 nm mean diameter, 250 nm height, and average interparticle separation of 650 nm. Note that unavoidable fabrication imperfections, such as surface roughness and fluctuations in the size and position of the particles (see the Supplemental Material [38] for more information), are deeply subwavelength and do not significantly influence the diffraction patterns measured using the customized optical setup shown in panel (c). IP denotes image plane, and AS denotes aperture stop. Measured (d),(e) and calculated (f),(g) intensity profiles of the prime arrays reported at the top of each column. The diffraction patterns (f) and (g) are calculated by considering more than 10^4 prime elements.

The computed structure factors are displayed in Figs. 1(f) and 1(g). We found a good agreement between the computed and the experimentally measured diffraction spectra, whose peaks are slightly broadened due to unavoidable fabrication imperfections. We have quantified these effects in the Supplemental Material [38], where we also provide a detailed analysis based on the comparison of the pair distribution functions of the arrays.

To demonstrate that the fluctuations of light scattered by the arrays exhibit strong multifractal properties, we apply the statistical approach proposed by Chhabra and Jensen [39] and implemented in the FRACLAC IMAGEJ software package [40]. This approach is based on the box-counting method that divides the space embedding an object into a hypercubic grid of boxes of varying size ϵ (see the Supplemental Material [38] for more details). We have computed three characteristic indicators of MF: (i) the generalized dimension $D(q)$, the mass exponent $\tau(q)$, and the multifractal spectrum $f(\alpha)$. The generalized dimension $D(q)$, first proposed as an alternative characterization of strange attractors of some dynamical systems, is defined as [41]

$$D(q) = \frac{1}{q - 1} \lim_{\epsilon \to 0} \left[\frac{\ln \mu(q, \epsilon)}{\ln \epsilon} \right], \qquad (2)$$
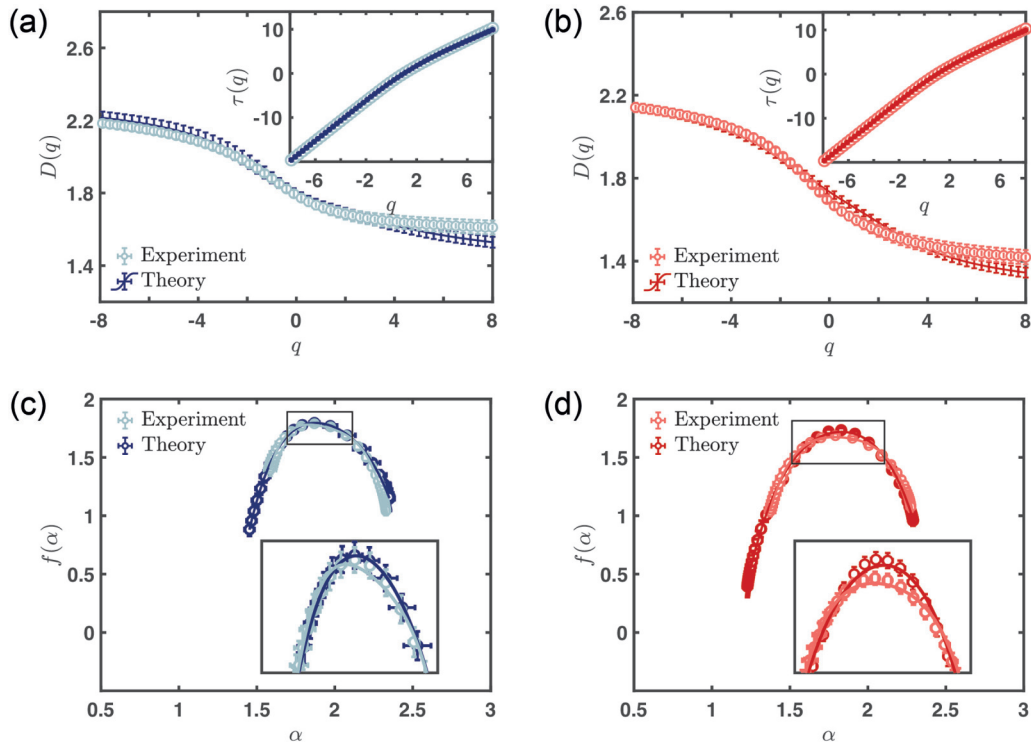
FIG. 2. $D(q)$ as a function of the moments q extrapolated from the measured (pastel-blue and pastel-red) and simulated (navy-blue and dark-red) scattered radiation from the Eisenstein (a) and Gaussian (b) arrays, respectively. The insets report the $\tau(q)$ exponents. Panels (c) and (d) show the $f(\alpha)$ spectra of the diffracted intensity of the Eisenstein and Gaussian array, respectively. Markers represent the data, while the continuous lines refer to the best fits obtained by using a least-squares method based on the polynomial function $f(\alpha) = p_1 + p_2\alpha + p_3\alpha^2 + p_4\alpha^3 + p_5\alpha^4$. Error bars take into account the different threshold percentages (between 55% and 75% of the maximum intensity value) used to binarize the diffraction patterns reported in Figs. 1(d)–1(g), as well as the different scaling methods used in the multifractal analysis [32].

where q are the moments of distribution, and the partition function $\mu(q, \epsilon)$ is equal to

$$\mu(q, \epsilon) = \sum_k P_k(\epsilon)^q \sim \epsilon^{-\tau(q)}. \qquad (3)$$

The probability $P_k(\epsilon)$ is evaluated as the integral of the measure over the kth box, and it scales as $P_k(\epsilon) \sim \epsilon^{\alpha_k}$. The coefficients α_k are the Lipschitz-Holder exponents, and they quantify the strength of the singularity of a given positive measure [39,41]. The mass exponent $\tau(q)$ describes the scaling of the partition function with respect to ϵ, and it defines $D(q)$ through the relation $D(q) = \tau(q)/(q - 1)$. Moreover, the Chhabra-Jensen method allows us to define the one-parameter family $\hat{\mu}_k(q, \epsilon)$ through the relation $\hat{\mu}_k(q, \epsilon) = P_k(\epsilon)^q / \sum_k P_k(\epsilon)^q$, such that the multifractal spectrum $f(\alpha)$ is obtained directly from the data by using the following expression:

$$f(\alpha) = \lim_{\epsilon \to 0} \frac{\sum_k \hat{\mu}_i(q, \epsilon) \ln[\hat{\mu}_i(q, l)]}{\ln \epsilon}. \qquad (4)$$

In particular, the numerator of Eq. (4) is evaluated for each moment q for decreasing box sizes. Then, $f(\alpha)$ is extrapolated from the slopes of $\sum_i \hat{\mu}_i(q, \epsilon) \ln[\hat{\mu}_i(q, \epsilon)]$ as a function of $\ln \epsilon$ [39].

Multifractal distributions are characterized by a smooth $D(q)$ function and a nonlinear dependence of τ from the moments q. These features are clearly visible in Figs. 2(a) and 2(b). Moreover, the singularity spectra reported in Figs. 2(c)

and 2(d) exhibit a downward concavity with a large width $\Delta\alpha$, which is the hallmark of multifractality [27,39]. The multifractal exponents extrapolated from the experimental data (lighter markers) follow well the ones estimated from the simulations (darker markers). Also note that multifractal spectra are global morphological properties of the diffraction spectra and are not influenced by the small local intensity fluctuations due to subwavelength fabrication imperfections, as we show in more detail in the Supplemental Material [38].

Even though little is known about the singularity spectrum from an analytical point of view [42], the shape of $f(\alpha)$ encodes information on the PDF of the quantity under investigation [43]. In particular, it is known that if $f(\alpha)$ is parabolic [i.e., well reproduced by the model $f(\alpha) = a + b\alpha + c\alpha^2$ with three free parameters], then the PDF follows a log-normal statistic (i.e., a model characterized by two free parameters; the mean and standard deviation) [27]. On the other hand, deviations of $f(\alpha)$ from a simple parabolic model reflect the non-Gaussian nature of its PDF [26,42–44]. In this case, we speak of strong-MF [43].

To better understand the multifractal properties of the diffraction intensity pattern of prime arrays, we have developed a nonparabolic model characterized by the polynomial function $f(\alpha) = p_1 + p_2\alpha + p_3\alpha^2 + p_4\alpha^3 + p_5\alpha^4$. This model [continuous lines in Figs. 2(c) and 2(d)] reproduces very well our data with an R^2-coefficient equal to 0.99 (see the Supplemental Material [38] for more details), demonstrating that photonic prime arrays exhibit strong-MF. Moreover, the
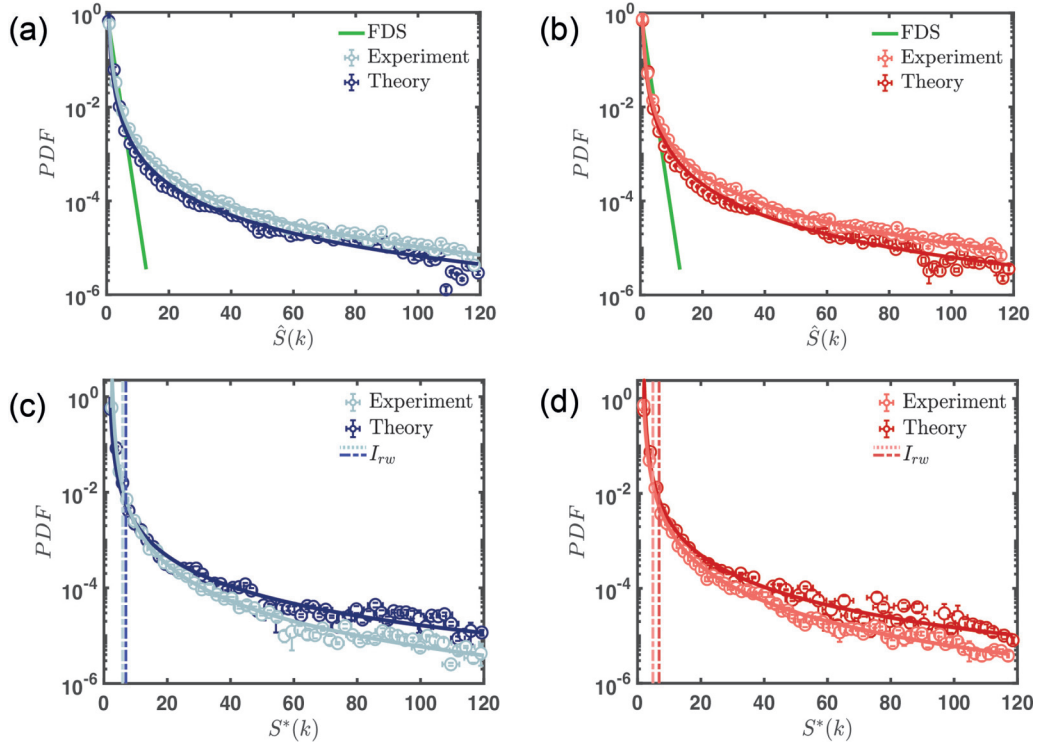
FIG. 3. Panels (a) and (b) display the PDFs of the fluctuations of the scattered radiation from the Eisenstein and Gaussian prime array. As a comparison, the negative exponential statistic of FDS, ensemble-averaged over 100 different uncorrelated arrangements of 2000 particles, is reported with a continuous green line. PDFs of the most intense light intensity fluctuations produced by the Eisenstein (c) and Gaussian (d) prime array. The dashed lines indicate the threshold values I_{RW}. Markers represent the data: pastel-blue and pastel-red markers express the measured data, while navy-blue and dark-red markers refer to the calculated intensities. Continuous lines in panels (a),(b) and (c),(d) refer, respectively, to the best fits of both measured and simulated data obtained by using a least-squares method based on Eqs. (5) and (6).

nonparabolicity of the $f(\alpha)$ spectra indicates that the associated PDFs are non-Gaussian distributions characterized by heavy tails.

III. MULTIFRACTALITY AND ROGUE WAVE FORMATION

To demonstrate the link between strong-MF and non-Gaussian PDFs of the fluctuation of light intensity, we evaluate the histograms of the array structure factor normalized with respect to its averaged value $\hat{S}(k) = S(k)/\overline{S}(k)$. Figures 3(a) and 3(b) show the results of this analysis extrapolated from the measured (lighter markers) and simulated (darker markers) data. In particular, these PDFs display remarkable heavy-tail features confirming the rogue wave character of the investigated far-field intensity profiles. The rare and extreme character of these distributions is particularly evident when compared against the negative exponential statistics $\exp[-\hat{S}(k)]$ (green continuous lines) that describes the fluctuations of waves scattered by uncorrelated random arrangements of particles, i.e., fully developed speckles (FDS) [45].

To quantify the observed heavy-tail behavior, we use a least-squares method based on the Pareto-type distribution defined as follows [46]:

$$P(x) = \frac{\beta}{\gamma \sigma}\left[1 + \left(\frac{x-\mu}{\sigma}\right)^{1/2\gamma}\right]^{-(\beta+1)}\left(\frac{x-\mu}{\sigma}\right)^{-1+1/\gamma}, \quad (5)$$

where $x = \hat{S}(k)$, while μ, σ, β, and γ are four free parameters named, respectively, the location, the scale, the shape, and the inequality exponent. The distribution (5) reproduces the experimental and simulation data very well with an R^2-coefficient almost equal to 0.99. These results, as discussed in more detail in the Supplemental Material [38], are robust with respect to the number of scatterers (up to 10^4) and to the exposure time used to measure the diffraction intensities reported in Figs. 1(d) and 1(e). The distributions of the Pareto family are α-stable distributions often used in EVT to model hazards in nature with long-range correlations, such as earthquakes, avalanches, rainfall distributions, the scaling laws of human travel, and financial crash markets [19,47–49]. Our findings demonstrate their applications to the optical regime by linking the multifractal properties of the scattered radiation of photonic arrays with the heavy-tailed PDF (5).

To demonstrate directly the optical rogue wave properties of the arrays, we compute histograms of the most intense fluctuations $S^*(k)$ and we evaluate the intensity threshold for rogue wave formation I_{RW} by using the oceanographic definition $I_{RW} \geqslant 2I_{1/3}$. The quantity $I_{1/3}$ indicates the mean intensity of the highest third of events [2]. The results are reported in Figs. 3(c) and 3(d), where the statistics extrapolated from the measured and simulated peak intensities are shown along with the intensity thresholds for rogue wave formation (dashed lines). The agreement between the statistics extracted from simulations (darker markers) and experiments

(lighter markers) is remarkable. Moreover, these distributions are characterized by heavy tails that exceed the threshold I_{RW}, demonstrating that the scattered radiation from the investigated arrays manifests the RW behavior. Concerning the probability of optical rogue wave events, Eisenstein and Gaussian prime arrays yield $3.6 \pm 0.95\%$ and $4.1 \pm 1.3\%$ of events [50]. Thanks to the multifractality of their geometrical structures, the proposed devices support a larger probability for optical rogue wave generation as compared to what is observed in linear systems that impart a random phase on a coherent optical field [7].

Finally, the continuous lines in Figs. 3(c) and 3(d) show that the distributions of the most intense fluctuations of the scattered intensities are well reproduced, with an R^2-coefficient almost equal to 0.98, by the distribution $G(x)$ defined as [19]

$$G(x) = \frac{1}{\rho}\left[1 + \xi\left(\frac{x-\tau}{\rho}\right)\right]^{-(1+1/\xi)}$$
$$\times \exp\left\{-\left[1 + \xi\left(\frac{x-\tau}{\rho}\right)\right]_+^{-1/\xi}\right\}, \qquad (6)$$

where $+$ indicates the constraint $[1 + \xi(\frac{x-\tau}{\rho})] > 0$, while ξ, ρ, and τ are the shape, the scale, and the location parameter, respectively. The probability density function (6) is the compact form of three widely used distributions in EVT, named Gumbel (primarily adopted in corrosion engineering to guarantee the safety of buildings and in meteorological phenomena), Fréchet (mostly utilized to model market returns), and Weibull (originally developed in materials science) [48]. In fact, the extremal types theorem, which is the analog of the central limit theorem in EVT, states that the distribution of the rescaled maxima of extreme events belongs to one of these three families [14,49]. Collectively, these three distributions are named extreme value distributions, and they can be parametrized into the single family distribution (6) known as the generalized extreme value distribution [14,49]. The shape parameter ξ discriminates the distribution class. $G(x)$ belongs to the Gumbel, to the Weibull, or to the Fréchet class, depending on whether ξ is equal to zero, lower than zero, or larger than zero, respectively. Moreover, a direct link exists between the distribution of extreme events $P(x)$ and the distribution of their most intense values $G(x)$ [14,19,48,49]. Such a link is particularly used in finance to predict the price movements characterized by independent and stationary increments, i.e., Lévy processes [48]. In particular, if $P(x)$ corresponds to the normal or exponential distribution, the distribution of the maxima values follows a Gumbel function. In cases in which $P(x)$ is characterized by a finite support (i.e., an upper end point such as the uniform and the beta

distribution), $G(x)$ approaches Weibull distribution. Lastly, $G(x)$ falls into the Fréchet class when $P(x)$ exhibits power-law (i.e., Pareto-type) tails [19,48,49]. The data of Figs. 3(c) and 3(d) are well-described for ξ values always larger than zero (see the Supplemental Material [38]), in agreement with the power-law features of the PDFs of panels (a) and (b). Interestingly, extreme value Fréchet distributions were observed in the statistics of natural hazards with long-term memory characteristics [19,48] and in the scaling behavior of focused waves in random media modeled as a Gaussian random field [15]. Our findings generalize these results to linear optical systems with strong multifractal behavior, introducing an alternative approach to achieve high-intensity optical hot spots.

IV. CONCLUSIONS

In conclusion, using the approach of extreme value theory, we demonstrated the formation of optical RWs with enhanced probability in multifractal arrays of dielectric nanoparticles based on the distributions of the prime elements in complex quadratic fields (prime arrays). Our findings link directly the strong multifractality of photonic prime arrays with intense RW phenomena in the linear optical regime. In particular, we developed a nonparabolic multifractal model that well-reproduces the experimentally measured multifractal spectra for the scattered radiation. The non-Gaussian PDFs of light intensity fluctuations associated with strong-multifractality have been characterized using heavy-tailed Pareto-type and Fréchet distribution for the most intense values, in excellent agreement with the experimental results. Notably, multifractality characterizes also oceanic rogue waves [31], suggesting a novel interpretation in the long-debated analogy between oceanographic and optical rogue waves. Our results unveil the key role of long-range structural correlations and strong-multifractality for the engineering of planar diffraction arrays that produce high-intensity RWs for applications to enhanced sensing and lithography.

[1] C. Kharif, E. Pelinovsky, and A. Slunyaev, *Rogue Waves in the Ocean* (Springer Science & Business Media, Berlin, 2008).

[2] J. M. Dudley, F. Dias, M. Erkintalo, and G. Genty, Nat. Photon. **8**, 755 (2014).

[3] J. M. Dudley, G. Genty, A. Mussot, A. Chabchoub, and F. Dias, Nat. Rev. Phys. **1**, 675 (2019).

[4] D. R. Solli, C. Ropers, P. Koonath, and B. Jalali, Nature (London) **450**, 1054 (2007).

[5] F. T. Arecchi, U. Bortolozzo, A. Montina, and S. Residori, Phys. Rev. Lett. **106**, 153901 (2011).

[6] R. Höhmann, U. Kuhl, H.-J. Stöckmann, L. Kaplan, and E. J. Heller, Phys. Rev. Lett. **104**, 093901 (2010).

[7] A. Mathis, L. Froehly, S. Toenger, F. Dias, G. Genty, and J. M. Dudley, Sci. Rep. **5**, 12822 (2015).

[8] A. Safari, R. Fickler, M. J. Padgett, and R. W. Boyd, Phys. Rev. Lett. **119**, 203901 (2017).

[9] Y. V. Bludov, V. V. Konotop, and N. Akhmediev, Phys. Rev. A **80**, 033610 (2009).

[10] P. Walczak, S. Randoux, and P. Suret, Phys. Rev. Lett. **114**, 143903 (2015).

[11] Y. Zhen-Ya, Commun. Theor. Phys. **54**, 947 (2010).

[12] V. Ruban, Y. Kodama, M. Ruderman, J. Dudley, R. Grimshaw, P. McClintock, M. Onorato, C. Kharif, E. Pelinovsky, T. Soomere *et al.*, Eur. Phys. J. Spec. Top. **185**, 5 (2010).

[13] K. Dysthe, H. E. Krogstad, and P. Müller, Annu. Rev. Fluid Mech. **40**, 287 (2008).

[14] S. Coles, *An Introduction to Statistical Modeling of Extreme Values* (Springer-Verlag, London, 2001), Vol. 208.

[15] J. J. Metzger, R. Fleischmann, and T. Geisel, Phys. Rev. Lett. **112**, 203903 (2014).

[16] C. Kharif and E. Pelinovsky, Eur. J. Mech. B **22**, 603 (2003).

[17] M. Onorato, S. Residori, U. Bortolozzo, A. Montina, and F. Arecchi, Phys. Rep. **528**, 47 (2013).

[18] G. Dematteis, T. Grafke, M. Onorato, and E. Vanden-Eijnden, Phys. Rev. X **9**, 041057 (2019).

[19] A. S. Sharma, A. Bunde, V. P. Dimri, and D. N. Baker, *Extreme Events and Natural Hazards: The Complexity Perspective* (AGU, Washington DC, 2013), Vol. 196.

[20] M. Berry, Proc. R. Soc. A **463**, 3055 (2007).

[21] J. F. Nye, *Natural Focusing and Fine Structure of Light: Caustics and Wave Dislocations* (IOP, Bristol, 1999).

[22] M. V. Berry and C. Upstill, in *Progress in Optics* (Elsevier, Amsterdam, 1980), Vol. 18, pp. 257–346.

[23] C. Bonatto, S. D. Prado, F. L. Metz, J. R. Schoffen, R. R. B. Correia, and J. M. Hickmann, Phys. Rev. E **102**, 052219 (2020).

[24] U. Frisch and G. Parisi, Ann. N.Y. Acad. Sci. **357**, 359 (1980).

[25] F. Schmitt, D. Schertzer, and S. Lovejoy, Int. J. Theor. Appl. Fin. **3**, 361 (2000).

[26] G. Paladin and A. Vulpiani, Phys. Rep. **156**, 147 (1987).

[27] T. Nakayama and K. Yakubo, *Fractal Concepts in Condensed Matter Physics* (Springer Science & Business Media, New York, 2013), Vol. 140.

[28] M. Soljacic, M. Segev, and C. R. Menyuk, Phys. Rev. E **61**, R1048 (2000).

[29] L. Telesca, A. Chamoli, M. Lovallo, and T. A. Stabile, Pure Appl. Geophys. **172**, 1933 (2015).

[30] T. Hirabayashi, K. Ito, and T. Yoshii, in *Fractals and Chaos in the Earth Sciences* (Springer, Berlin, 1992), pp. 591–610.

[31] A. Hadjihosseini, M. Wächter, N. P. Hoffmann, and J. Peinke, New J. Phys. **18**, 013017 (2016).

[32] F. Sgrignuoli, S. Gorsky, W. A. Britton, R. Zhang, F. Riboli, and L. Dal Negro, Commun. Phys. **3**, 106 (2020).

[33] R. Wang, F. A. Pinheiro, and L. Dal Negro, Phys. Rev. B **97**, 024202 (2018).

[34] S. Lang, *Algebraic Number Theory*, 2nd ed. (Springer, New York, 1994).

[35] T. J. Dekker, CWI Quarterly **7**, 367 (1994).

[36] M. Wolf, Physica **160**, 24 (1989).

[37] J. W. Goodman, *Introduction to Fourier Optics* (Roberts & Co., Greenwood Village, CO, 2005).

[38] See Supplemental Material at http://link.aps.org/supplemental/10.1103/PhysRevB.103.195403 for additional details on the samples fabrication and characterization as well as extended discussions on the multifractal and rogue waves analysis.

[39] A. Chhabra and R. V. Jensen, Phys. Rev. Lett. **62**, 1327 (1989).

[40] C. A. Schneider, W. S. Rasband, and K. W. Eliceiri, Nat. Methods **9**, 671 (2012).

[41] P. Grassberger and I. Procaccia, Phys. Rev. Lett. **50**, 346 (1983).

[42] L. J. Vasquez, A. Rodriguez, and R. A. Römer, Phys. Rev. B **78**, 195106 (2008).

[43] A. Rodriguez, L. J. Vasquez, and R. A. Römer, Phys. Rev. Lett. **102**, 106406 (2009).

[44] B. B. Mandelbrot, in *Statistical Models and Turbulence* (Springer, Berlin, 1972), pp. 333–351.

[45] J. W. Goodman, *Statistical Optics* (Wiley, Hoboken, NJ, 2015).

[46] B. C. Arnold, Wiley StatsRef: Statistics Reference Online, 1 (2014).

[47] D. Brockmann, L. Hufnagel, and T. Geisel, Nature (London) **439**, 462 (2006).

[48] F. Longin, *Extreme Events in Finance: A Handbook of Extreme Value Theory and Its Applications* (Wiley, Hoboken, NJ, 2016).

[49] M. R. Leadbetter, G. Lindgren, and H. Rootzén, *Extremes and Related Properties of Random Sequences and Processes* (Springer-Verlag, New York, 2012).

[50] The probability of rogue wave formation extracted from the simulations is compatible with the measured values, i.e., $(2.9 \pm 1.4)\%$ for the Eisenstein and $(3.4 \pm 1.4)\%$ for the Gaussian prime array. See also the supplemental material [38], which also includes Ref. [51].

[51] J. Zheng, S. Bao, Y. Guo, and P. Jin, Surf. Coat. Technol. **240**, 293 (2014).